





Generating high-order exceptional points in coupled electronic oscillators using complex synthetic gauge fields

José D. Huerta-Morales ^{1,*} Mario A. Quiroz-Juárez ² Yogesh N. Joglekar ^{3,†} and Roberto de J. León-Montiel ^{1,‡}

¹*Instituto de Ciencias Nucleares, Universidad Nacional Autónoma de México, Apartado Postal 70-543, 04510 Cd. Mx., México*

²*Centro de Física Aplicada y Tecnología Avanzada, Universidad Nacional Autónoma de México, Boulevard Juriquilla 3001, 76230 Querétaro, México*

³*Department of Physics, Indiana University–Purdue University Indianapolis (IUPUI), Indianapolis, Indiana 46202, USA*



(Received 13 February 2023; revised 6 April 2023; accepted 14 April 2023; published 24 April 2023)

Exceptional points (EPs) are degeneracies of non-Hermitian systems, where both eigenvalues and eigenvectors coalesce. Classical and quantum systems exhibiting high-order EPs have recently been identified as fundamental building blocks for the development of novel, ultrasensitive optoelectronic devices. However, arguably one of their major drawbacks is that they rely on nonlinear amplification processes that could limit their potential applications, particularly in the quantum realm. In this work, we show that high-order EPs can be designed by means of linear, time-modulated, chain of inductively coupled RLC (where R stands for resistance, L for inductance, and C for capacitance) electronic circuits. With a general theory, we show that N coupled circuits with $2N$ dynamical variables and time-dependent parameters can be mapped onto an N -site, time-dependent, non-Hermitian Hamiltonian, and obtain constraints for \mathcal{PT} symmetry in such models. With numerical calculations, we obtain the Floquet exceptional contours of order N by studying the energy dynamics in the circuit. Our results pave the way toward realizing robust, arbitrary-order EPs by means of synthetic gauge fields, with important implications for sensing, energy transfer, and topology.

DOI: [10.1103/PhysRevA.107.042219](https://doi.org/10.1103/PhysRevA.107.042219)

I. INTRODUCTION

The past two decades have witnessed a Cambrian explosion of several experimental and theoretical investigations on non-Hermitian Hamiltonian systems that satisfy the so-called parity-time (\mathcal{PT}) symmetry condition [1–5]. Owing to the antilinear \mathcal{PT} symmetry, the spectrum of such Hamiltonians changes from real to complex-conjugate pairs as the degree of anti-Hermiticity is increased. The coherent, nonunitary evolution generated by the non-Hermitian Hamiltonian means that the norm of a state oscillates in the \mathcal{PT} -symmetric region, where the spectrum is real, and grows exponentially in the \mathcal{PT} -broken region, where amplifying (and decaying) eigenmodes are present. The study and analysis of \mathcal{PT} -symmetric systems across the parameter domain have triggered important theoretical predictions and experimental demonstrations in disparate areas of physics, optics, and photonics [6–9]. Specifically, the nontrivial phenomena across the \mathcal{PT} transition have captured a great deal of attention. This is, in part, because the exceptional-point degeneracy—in contrast with the traditional Hermitian degeneracy—is a potentially good candidate for sensing small disturbances due to a perturbing potential [10–16].

For Hermitian Hamiltonians, however, even when two eigenvalues become degenerate, two orthonormal

eigenvectors remain. Exceptional points (EPs) are thus non-Hermitian singularities where two or more eigenvectors also coalesce [17–19]. The number of eigenvectors n that collapse at the non-Hermitian degeneracy defines the order of the EP, and we call it EP n . The most common case is an EP2, where a pair of eigenvalues become degenerate, and EPs of order greater than two are traditionally referred to as high-order EPs [20–23]. The literature on the design and realization of high-order EPs has greatly contributed to the development of this research field, most of them aimed at enhancing the response of open physical systems [24,25] because the dimensionless mode-splitting $\Delta\omega$ in response to a dimensionless perturbation $\delta \ll 1$ at an EP n is given by $\Delta\omega(\delta) \propto \delta^{1/n} \gg \delta$. Put simply, the sensitivity to perturbations increases as the order of the EP increases. For instance, a 1% perturbation results in a 1% response in a Hermitian system, a 10% response at an EP2, and a 30% response at an EP3.

Recent theoretical and experimental studies have focused on diverse \mathcal{PT} -symmetric platforms to realize EPs of arbitrary order. Examples include waveguide arrays [7,9,26], microcavities [13,14,27], optomechanical systems [28–30], quantum optical circuits [31,32], coupled acoustic resonators [33–35], and electronic circuits [12,36–39]. The latter, in recent years, have emerged as a powerful platform for simulating topological and non-Hermitian phenomena [40–42]. In particular, we have shown that both gain and loss can be implemented in a single LC oscillator by means of complex, synthetic gauge fields, thereby creating static and Floquet EP2 landscape [43]. Extending this approach to higher-dimensional EPs is, however, nontrivial.

*jose.huerta@correo.nucleares.unam.mx

†yojoglek@iupui.edu

‡roberto.leon@nucleares.unam.mx

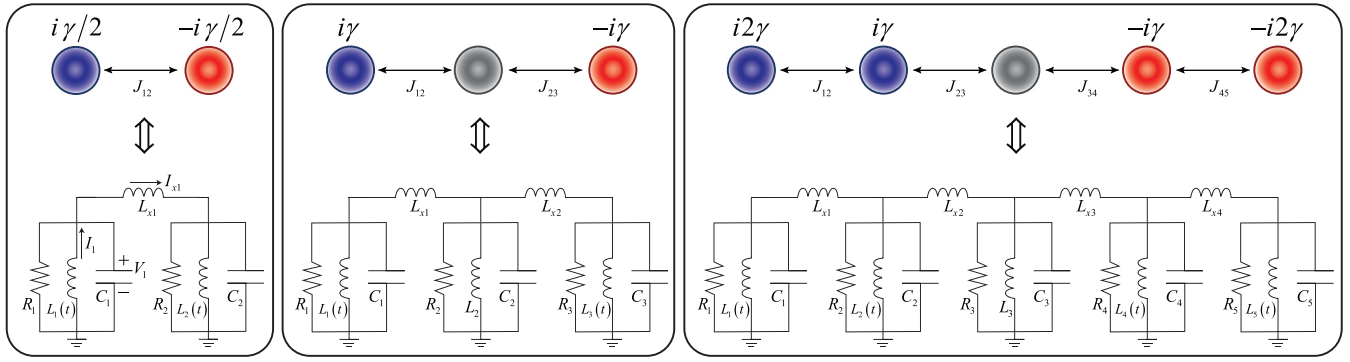


FIG. 1. Schematic representation of the equivalence between sites and electronic circuits in a tight-binding lattice model. The top row shows \mathcal{PT} -symmetric perfect-state-transfer lattice with $N = 2, 3, 5$ sites, respectively. Its Hamiltonian $H_N(\gamma) = \kappa J_y + i\gamma J_z$ is N dimensional. Bottom row shows N inductively coupled RLC circuits with $2N$ dynamical variables, exhibiting synthetic gain and loss by means of time-dependent inductance within each RLC box. Note that, for the sake of clarity, we have labeled the voltage V_1 , current I_1 and current $I_{x,1}$ present in the capacitor, inductor and coupling inductor, respectively, of the first RLC circuit (left panel). This labeling can be generalized to the whole circuit by drawing the corresponding voltages and currents for each oscillator.

In this work, we show through analytical and numerical methods that it is possible to engineer high-order EPs in an inductively coupled RLC-circuit tight-binding lattice. We use the J_y array—a tight-binding lattice with nonuniform couplings that has equidistant eigenvalues [44–46]—along with a gain-loss profile that mimics the J_z array to realize higher-order EPs [19]. Specifically, we implement the non-trivial features of \mathcal{PT} symmetry with synthetic gain and loss through the temporal variation of the inductances in each oscillator [38,39,43]. Our results suggest that dynamically tunable synthetic electronics, with \mathcal{PT} symmetry implemented through a complex gauge field, can be used to simulate higher-order EPs.

The paper is organized as follows. In Sec. II we present the formalism that maps the Kirchoff-law equations for currents and voltages in a chain of N inductively coupled RLC oscillators into a Schrodinger-like equation with a $N_e \equiv (3N - 1)$ -dimensional Hamiltonian, and show how a time-dependent, nonunitary change of basis can lead to gain and loss. In Sec. III we demonstrate that the time modulation of specific components of those oscillators can create EPN contours. Section IV provides a brief discussion and conclusions. The explicit forms of the Hamiltonians for $N = 3, 4, 5$ are given in the Appendix.

II. THE MODEL

Let us consider a set of N RLC circuits connected by $(N - 1)$ coupling inductors (Fig. 1). Their dynamics are governed by the following first-order equations [47]:

$$\frac{dV_n}{dt} = \frac{1}{C_n} \left[-\frac{V_n}{R_n} - I_n - I_{x,n} + I_{x,n-1} \right], \quad (1a)$$

$$\frac{dI_n}{dt} = \frac{1}{L_n} V_n, \quad (1b)$$

$$\frac{dI_{x,n}}{dt} = \frac{1}{L_{x,n}} (V_n - V_m). \quad (1c)$$

These equations arise from the Kirchoff laws. Here, $V_n(t)$ is the voltage in the capacitor C_n , $I_n(t)$ is the current across

the inductor L_n , R_n is the resistance in the n th oscillator, $L_{x,n}$ denotes the inductor coupling the n th RLC box to the $(n+1)$ th box, and $I_{x,n}(t)$ is the current flowing across it. We can write the $N_e \equiv (3N - 1)$ Eqs. (1a)–(1c) in a compact form as

$$i \frac{d}{dt} |\phi(t)\rangle = H(t) |\phi(t)\rangle, \quad (2)$$

where the N_e -dimensional “state vector” is

$$|\phi(t)\rangle = (V_1, \dots, V_N, I_1, \dots, I_N, I_{x,1}, \dots, I_{x,N-1})^T, \quad (3)$$

$H(t)$ is a non-Hermitian, $N_e \times N_e$ matrix with purely imaginary entries. To specify its general structure, we define ancillary matrices $\mathbb{C} = \text{diag}(C_1, \dots, C_N)$, $\mathbb{L} = \text{diag}(L_1, \dots, L_N)$, $\mathbb{G}_{RC} = \text{diag}(1/R_1 C_1, \dots, 1/R_N C_N)$, and $\mathbb{L}_x = \text{diag}(L_{x,1}, \dots, L_{x,N-1})$. Additionally, we also define an $N \times (N - 1)$, almost skew-symmetric matrix \mathbb{S} with entries $\mathbb{S}_{ab} = \delta_{ab} - \delta_{a,b+1}$. In terms of these matrices, H can be written as

$$H = i \begin{bmatrix} -\mathbb{G}_{RC} & -\mathbb{C}^{-1} & -\mathbb{C}^{-1}\mathbb{S} \\ \mathbb{L}^{-1} & 0 & 0 \\ \mathbb{L}_x^{-1}\mathbb{S}^\dagger & 0 & 0 \end{bmatrix}. \quad (4)$$

Since the state vector $|\phi(t)\rangle$ has entries with different engineering dimensions, so does the matrix H . To clarify its underlying symmetry properties, it is useful to consider the “square-root-of-energy” basis. The energy in the N -node circuit is given by

$$\begin{aligned} E(t) &= \frac{1}{2} \sum_{n=1}^N [C_n V_n^2 + L_n I_n^2] + \frac{1}{2} \sum_{m=1}^{(N-1)} L_{x,m} I_{x,m}^2 \\ &= \langle \phi(t) | A | \phi(t) \rangle, \end{aligned} \quad (5)$$

where the positive, N_e -dimensional bilinear-form matrix is given by $A = \text{diag}(\mathbb{C}, \mathbb{L}, \mathbb{L}_x)/2$. We define $|\psi(t)\rangle = A^{1/2}(t)|\phi(t)\rangle$ so that norm of $|\psi(t)\rangle$ encodes the circuit energy, $\langle \psi(t) | \psi(t) \rangle = E(t)$. Note that all entries in the state vector $|\psi(t)\rangle$ have units of $\sqrt{\text{Joules}}$. It is straightforward to

show that $|\psi(t)\rangle$ satisfies a Schrödinger-like equation,

$$i \frac{d}{dt} |\psi(t)\rangle = (H_0 + \Gamma) |\psi(t)\rangle = H_{\text{cir}}(t) |\psi(t)\rangle, \quad (6)$$

where the effective circuit Hamiltonian $H_{\text{cic}} = H_0 + \Gamma$ has two components. The first component H_0 is given by

$$H_0 = \sqrt{AH} \frac{1}{\sqrt{A}} = i \begin{bmatrix} -\mathbb{G}_{RC} & -\mathbb{W} & -\frac{1}{\sqrt{C}} \mathbb{S} \frac{1}{\sqrt{L_x}} \\ \mathbb{W} & 0 & 0 \\ \frac{1}{\sqrt{L_x}} \mathbb{S}^\dagger \frac{1}{\sqrt{C}} & 0 & 0 \end{bmatrix}, \quad (7)$$

where $\mathbb{W} = \text{diag}(\omega_1, \dots, \omega_N)$ is a diagonal matrix with frequencies of individual oscillators $\omega_k = 1/\sqrt{C_k L_k}$. When there is no dissipation in each RLC circuit, i.e., $\mathbb{G}_{RC} = 0$, the matrix H_0 becomes Hermitian and the corresponding unitary evolution of the state $|\psi(t)\rangle$ signals the conservation of total energy in the circuit. When $\mathbb{G}_{RC} > 0$, this anti-Hermitian piece of H_0 encodes the Joule dissipation.

The second component of H_{cic} corresponds to a complex gauge potential given by [43]

$$\Gamma(t) = i \frac{1}{\sqrt{A}} \frac{d}{dt} \sqrt{A} = i \frac{d}{dt} \ln \sqrt{A(t)}. \quad (8)$$

Traditionally, ‘‘gauge potential’’ denotes the change in the Hamiltonian (or Lagrangian) resulting from spatiotemporal variation in the change of basis. In its most common manifestation, when the wave function of a charged particle is multiplied by a phase factor, $\psi(x) \rightarrow \psi'(x) \equiv \exp[ie \int^x \mathbf{A} \cdot d\mathbf{r}/(\hbar c)] \psi(x)$, the momenta get a correction, $-i\hbar\nabla \rightarrow -i\hbar\nabla - e\mathbf{A}/c$, that is the logarithmic derivative of the unitary $U_{x,x'} = \delta_{x,x'} \exp[ie \int^x \mathbf{A} \cdot d\mathbf{r}/(\hbar c)]$ for the change $\psi \rightarrow \psi'$. If the change of basis matrix $\sqrt{A(t)}$ is unitary, as is typically the case, its spatiotemporal variations give rise to a Hermitian $\Gamma(t)$ since the logarithm of a unitary matrix is an anti-Hermitian matrix. However, as our change of basis matrix $A = \text{diag}(\mathbb{C}, \mathbb{L}, \mathbb{L}_x)/2$ is not unitary and always real, it leads to an anti-Hermitian, gain-loss gauge term $\Gamma(t)$, as defined in Eq. (8).

The parity operator exchanges the node n with its mirror symmetric node $\bar{a} = N + 1 - a$. Therefore, it is given by $\mathcal{P} = \text{diag}(\Pi_N, \Pi_N, -\Pi_{N-1})$ where $\Pi_k = \Pi_k^{-1} = \Pi_k^\dagger$ is the anti-diagonal matrix of size k with unit entries. The time-reversal operator, in addition to the complex-conjugation operation $*$, reverses the sign of each current: $\mathcal{T} = \text{diag}(\mathbb{1}_N, -\mathbb{1}_N, -\mathbb{1}_{N-1})*$. Thus, the antilinear \mathcal{PT} operator is given by the following N_e -dimensional, block-diagonal matrix,

$$\mathcal{PT} = \text{diag}(\Pi_N, -\Pi_N, \Pi_{N-1}) * = \mathcal{U} *, \quad (9)$$

where \mathcal{U} denotes the N_e -dimensional real, unitary matrix. By imposing the constraint that H_0 is \mathcal{PT} symmetric, we get

$$\Pi_N \mathbb{G}_{RC} \Pi_N = -\mathbb{G}_{RC} = 0, \quad (10)$$

$$\Pi_N \mathbb{W} \Pi_N = \mathbb{W}, \quad (11)$$

$$\Pi_N \frac{1}{\sqrt{C}} \mathbb{S} \frac{1}{\sqrt{L_x}} = \frac{1}{\sqrt{C}} \mathbb{S} \frac{1}{\sqrt{L_x}} \Pi_{N-1}. \quad (12)$$

Equivalently, these conditions mean no resistive losses, $\omega_a = \omega_{\bar{a}}$, and $C_a L_{x,a} = C_{\bar{a}} L_{x,\bar{a}}$. Similarly, requiring \mathcal{PT} symmetry for the anti-Hermitian potential implies $\mathcal{PAP} = A$ or equivalently, $C_a = C_{\bar{a}}$, $L_a = L_{\bar{a}}$, and $L_{x,a} = L_{x,N-a}$.

Next, we outline the mapping of this N_e -dimensional dynamical system onto an N -dimensional tight-binding model. Since H_0 has purely imaginary entries, for a \mathcal{PT} -symmetric Hamiltonian, the unitary \mathcal{U} in Eq. (9) anticommutes with it. Therefore, the eigenvalues of H_0 occur in pairs $\pm\epsilon_a$, or equivalently, it has a chiral symmetry. It also follows, most clearly from Eq. (7), that H_0 has $(N - 1)$ linearly dependent columns and therefore $(N - 1)$ eigenvalue zeros. This combination of chiral symmetry and zero modes is instrumental to mapping the $N_e = (3N - 1)$ dimensional system onto an N -dimensional model. These arguments remain valid when a \mathcal{PT} -symmetric complex gauge potential Γ is added, and therefore, the \mathcal{PT} -symmetric circuit Hamiltonian H_{cic} of size N_e can always be mapped onto a \mathcal{PT} -symmetric tight-binding model with N sites.

The canonical model with an EP of order N is $H(\gamma) = \kappa J_x + i\gamma J_z$ where J_x, J_z are N -dimensional representations of $\text{SU}(2)$ [19,21,44,48]. However, because we have a classical system with a purely real state vector, we use its counterpart with purely imaginary entries, $H_N(\gamma) = \kappa J_y + i\gamma J_z$. In such tight-binding lattice, the Hermitian coupling between adjacent sites is given by $J_y(a, a + 1) = i\sqrt{a(N + 1 - a)}/2 = -J_y(a + 1, a)$. Now, to connect the J_y matrix elements to our coupled electrical circuits model, we use the expression for the effective, dimensionless tunneling amplitude between two inductively coupled circuits, $J_{\text{eff}} = M^2/2\sqrt{1 + M^2}$ where $M^2 = L/L_x$ [49].

Similarly, to create the gain-loss term $i\gamma(t)J_z$ the inductors $L_a(t)$ within each circuit are modulated while keeping the capacitors and coupling inductors static across the array. Since $J_z = \text{diag}(s, s - 1, \dots, -s)$ where $s = (N - 1)/2$ is the spin associated with the N -dimensional representation, using the modulation,

$$L_a(t) \equiv L_0 e^{f_a(t)} = L_0 e^{(N+1-2a) \int_0^t \gamma(t') dt'}, \quad (13)$$

leads to a complex synthetic gauge potential $\Gamma = i\gamma(t) \text{diag}(0_N, J_z, 0_{N-1})$. This temporal variation means the inductors in mirror-symmetric positions are varied in an inverse manner, $L_a(t)L_{\bar{a}}(t) = L_0^2 = \text{const}$. Therefore, when inductance increase at site a , indicating gain, is balanced by inductance decrease at its mirror symmetric site \bar{a} , indicating loss, and \mathcal{PT} symmetry can be created without real amplifying or Joule-heating elements. The exponent function $f(t) = \int \gamma(t') dt'$ in Eq. (13) allows us to create arbitrary, balanced gain-loss profiles.

The choice of $f(t)$ is informed by the ability to dynamically modulate the synthetic inductances in real time by using electronic circuits [43]. Creating a static gain-loss term requires inductances that either grow or decay exponentially [43]. However, Floquet EP contours of the same order also emerge by periodic variations [43,49,50]. For simplicity, we consider the square-wave function,

$$f(t) = \begin{cases} \alpha & 0 \leq t \leq T/4, \\ -\alpha & T/4 < t < 3T/4, \\ \alpha & 3T/4 < t \leq T, \end{cases} \quad (14)$$

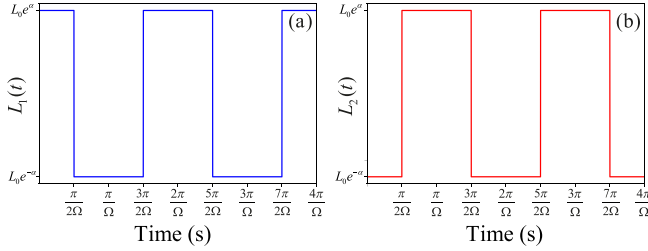


FIG. 2. Square-wave periodic function with modulation frequency Ω . (a) For $N = 2$, the time-dependent inductances are given by $L_1(t) = L_0 e^{f(t)}$. (b) The complementary, $L_2(t) = L_0 e^{-f(t)} = L_0^2/L_1(t)$.

where T is the period and $\Omega = 2\pi/T$ defines the modulation frequency. For example, when $N = 2$, the two inductances satisfy $e^{-\alpha} \leq L_{1,2}(t)/L_0 \leq e^{\alpha}$ (Fig. 2). Since the inductance in each RLC box varies with time, the Hamiltonian H_0 also acquires time dependence through the matrix \mathbb{W} of frequencies $\omega_a(t) = 1/\sqrt{L_a(t)C_a}$.

The \mathcal{PT} phase diagram of this system can be obtained via two methods. The first uses the nonunitary time evolution operator $G_F(T)$ to calculate the equivalent non-Hermitian, \mathcal{PT} -symmetric Floquet Hamiltonian $G_F(T) \equiv \exp[-iH_F(\alpha, \Omega)T]$ [50]. The second, experimentally friendly approach is to obtain the time-dependent circuit energy $E(t)$, Eq. (5), and compare its growth over sufficiently long time intervals τ and 2τ . To quantify it, we define a dimensionless ratio [43,49]:

$$\mu = \ln \left\{ \frac{\max [E(0 \leq t \leq 2\tau)]}{\max [E(0 \leq t \leq \tau)]} \right\}. \quad (15)$$

In the \mathcal{PT} -symmetric phase with time-periodic dynamics, $\max E(t)$ will be the same over the two intervals, and therefore $\mu = 0$ denotes the \mathcal{PT} -symmetric phase. On the other hand, in the \mathcal{PT} -broken phase with exponentially amplifying modes, Eq. (15) provides a linear-in- τ metric that indicates the average amplification $\mu > 0$. The \mathcal{PT} transition is accompanied by a vanishing energy gap and divergent period on the \mathcal{PT} -symmetric side of the boundary. Therefore, at any finite τ , this approach leads to some smearing of the EP contours. In the following section, we present the results of such an analysis.

III. RESULTS

For numerical analysis, we use experimentally accessible and viable circuit parameters [43]: resistance $R_0 = 1$ k Ω , inductance $L_0 = 0.01$ H, and capacitance $C_0 = 100$ μ F. Thus, the isolated oscillator frequency is $\omega_0/(2\pi) = 159.15$ Hz, and the isolated oscillator RC-decay rate, $1/R_0C_0 = 10$ Hz, is much smaller than the natural frequency, thereby justifying the approximation $\mathbb{G}_{RC} \approx 0$. The coupling inductances are set to $L_{x1} = 0.5L_0$ for $N = 2$ oscillators, $L_{x1} = L_{x2} = 0.5L_0$ for $N = 3$ oscillators, and $L_{x1} = L_{x4} = 0.67L_0$, $L_{x2} = L_{x3} = 0.5L_0$ for $N = 5$ as necessitated by the nonuniform matrix elements of the J_y array. We use $\alpha \leq 0.4$, meaning the inductances span $0.67L_0 \leq L_a(t) \leq 1.5L_0$, a range that can be dynamically achieved in the synthetic circuits [43,49].

The left-hand panel in Fig. 3 shows the numerically computed $\mu(\alpha, \Omega)$ for $N = 5$ [Fig. 3(a)], $N = 3$ [Fig. 3(b)], and $N = 2$ [Fig. 3(c)] over a modulation-frequency window $\Omega/(2\pi)$ from 300 to 600 Hz. The dark regions with $\mu = 0$ denote the \mathcal{PT} -symmetric phase, where the circuit energy $E(t)$ undergoes bounded oscillations. They are punctuated by bright, triangular, \mathcal{PT} -symmetry broken regions ($\mu > 0$) that occur down to vanishingly small non-Hermiticity $\alpha \ll 1$ at specific frequencies [43,49,50]. These regions are separated by EP contours with order N .

We analyze the dynamics at the EPs by monitoring how fast the circuit energy $E(t)$ increases when the system is parked at the EPs (shown by blue, left and purple, right circles with white boundaries) along $\alpha = \{0.2, 0.3, 0.4\}$ lines. The center panel in Fig. 3 shows normalized energies $E(t)/E_{\max}$ (solid lines) and their respective stroboscopic results (black-dashed lines) at $\alpha = 0.4$ [Fig. 3(d)], $\alpha = 0.3$ [Fig. 3(e)], and $\alpha = 0.2$ [Fig. 3(f)] when the system is parked on the blue, left-hand side EPs. Figures 3(g)–3(i) show corresponding results when the system is parked on the purple, right-hand side EPs. In each case, it can be seen that $E(t)/E_{\max}$ follows a power-law dependence on t with an exponent that increases with the order of the EP. This result is independent of the degree of non-Hermiticity α or the location—left or right—of the EP contour. The large fluctuations in the nonstroboscopic data for $E(t)$ also hint at the asymmetric dependence of $E(t)$ on the EP location at a fixed α [43].

Since the system with N has an N th order EP, we expect the unnormalized energy to grow as $E(t) \propto t^{2(N-1)}$ at long times. To confirm this, Fig. 4 shows the system's energy vs time on a log-log scale for $\alpha = 0.2$ at right-hand side EPs. The slopes obtained from straight-line fits to the log-log data are in agreement with the prediction that the power-law exponent for an EP of order N is given by $2(N-1)$ [21,43].

Some comments concerning the potential challenges in implementing electrical circuits of Fig. 1 are in order. One could try to construct coupled LC oscillators using passive components. However, this approach is typically constrained by the substantial damping coefficient in the inductor, which results in rapid energy dissipation, thereby impeding the detection of the desired effects. Furthermore, the implementation of time-dependent parameters often requires fluctuations in the physical properties of the circuit elements, which may not always be feasible.

A better potential option is to construct active electrical networks consisting of resistors, capacitors, and operational amplifiers. These elements can be interconnected in a specific way to synthesize differential equations. Interestingly, it has recently been shown that a single LC oscillator with both gain and loss can be implemented by means of active electrical networks with temporal modulation of their parameters [43]. One significant benefit of this approach is the potential to utilize analog multipliers to replace physical components that represent system parameters. This configuration allows the parameter values to be determined by external voltage sources, so the features of parameter modulation dependent on the waveform of the external signal.

In an ideal scenario, analog multipliers can be constructed using operational amplifiers and diodes. However, it is important to note that diodes are temperature dependent and

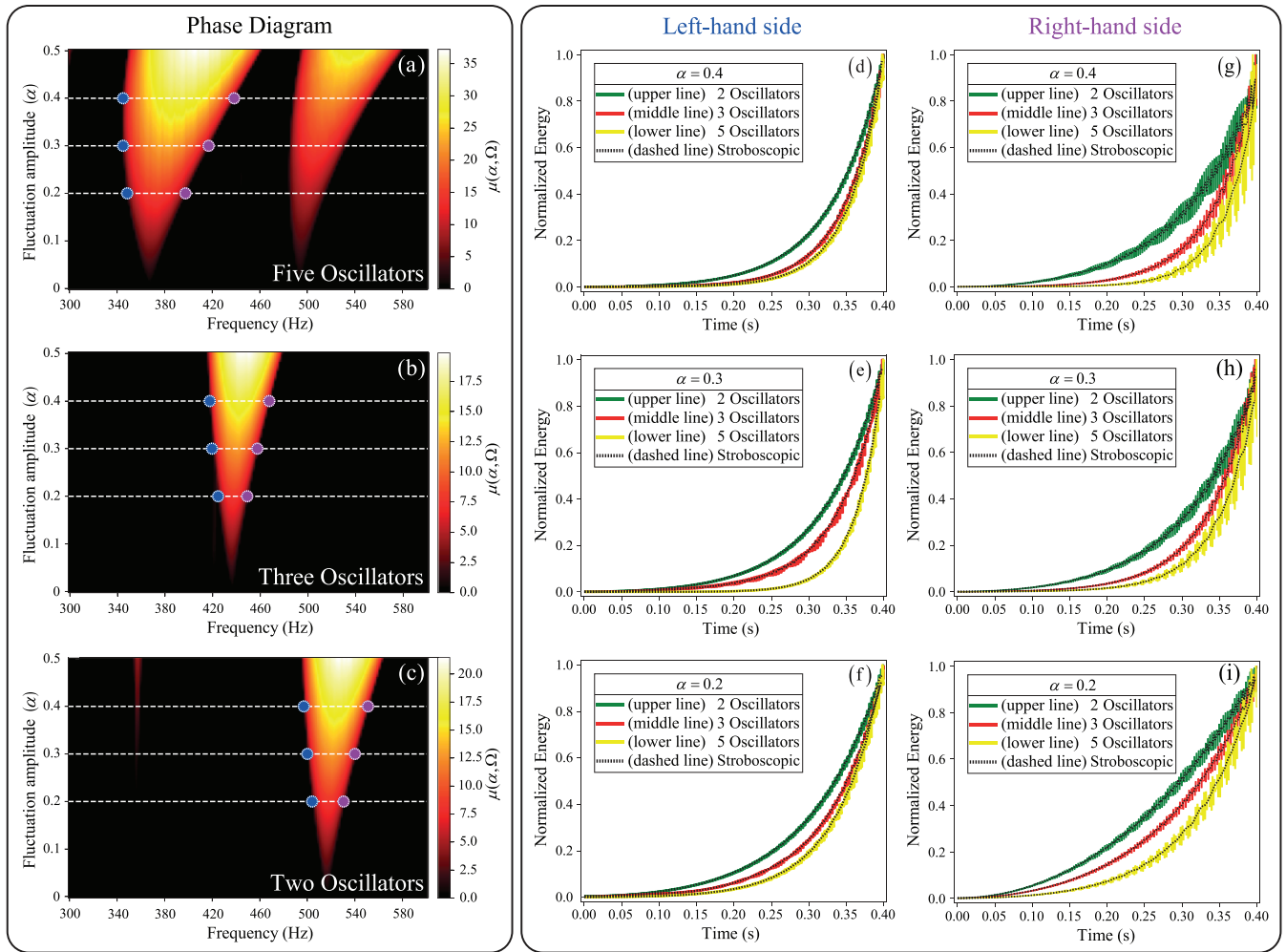


FIG. 3. High-order EP contours in the (α, Ω) plane. (a)–(c) $\mu(\alpha, \Omega)$ in the frequency window from $\Omega/(2\pi) = 300\text{--}600$ Hz is obtained using $\tau = 100$ ms. The EP contours, separating regions from light windows, are clearly seen, with EPs along the $\alpha = \{0.2, 0.3, 0.4\}$ lines shown as blue (left) and purple (right) solid circles. (d)–(f) Normalized energy $E(t)/E_{\max}$ for blue EPs on the left-side contour shows power law in time growth, with an exponent determined by N , but independent of α . Results for two, three, and five oscillators are shown in green (upper), red (middle), and yellow (lower) lines, respectively; overlaid black-dashed lines show stroboscopic results. (g)–(i) Corresponding results for the purple EPs on the right-side contour, shown with the same conventions, are quantitatively similar.

their characteristics can vary significantly from one diode to another, even within the same manufacturing batch. Consequently, it is important to consider integrated devices that include internal compensations for temperature variations so as to create stabilized multiplication operations. Another potential challenge in the implementation of electronic circuits for engineering high-order exceptional points is unavoidable losses present in electronic circuits. As one might expect, the energy of each individual oscillator in the presence of losses (or resistance) decays exponentially, with a rate $\gamma = 1/(RC)$. Experimental studies [47,49] have shown that the total resistance of the circuit can be quantified, thus making it feasible to design circuits that facilitate the observation of the sought-after effects. In order to minimize poor contacts and high variability in passive components, it is convenient to mount and solder electronic devices on a printed circuit board and use components with minimal tolerance. A stabilized voltage source to power the electronic circuit should also be used in order to prevent fluctuations in the bias voltage applied to the

operational amplifiers. This is important because the output of these devices is sensitive to the bias voltage.

Finally, we conclude this section by remarking that a significant feature of using electronic circuits is that the energy history of the system can be traced by experimentally monitoring the temporal evolution of voltages and currents through an oscilloscope. As depicted in Fig. 4, one can thus use that information to determine the order of the exceptional point by quantifying the rate at which the system's energy grows.

IV. CONCLUSION

From their start in quantum theory and mathematical physics, non-Hermitian, \mathcal{PT} -symmetric models are now studied across the board in fields as widely varied as minimal quantum systems or a single LC oscillator. This veritable cornucopia of experimental realizations has also invited detailed comparison of seemingly different models. Here, we have analyzed one such model, an array of N inductively

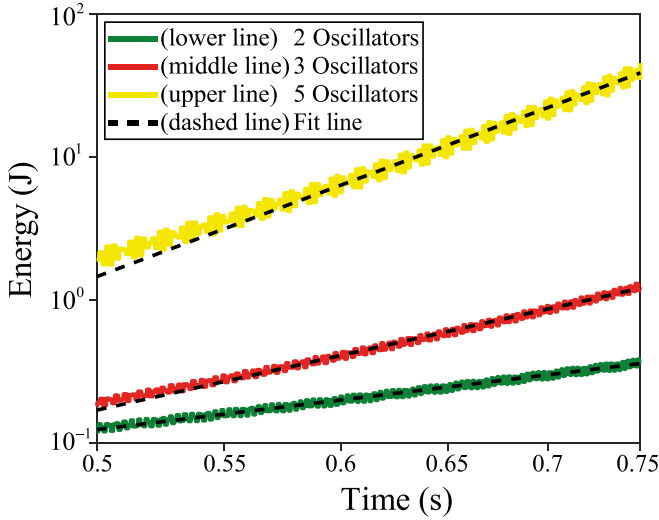


FIG. 4. Energy increase at the EPs. Unnormalized circuit energy $E(t)$ on a log-log scale at long times shows linear behavior with a slope that depends on the order N of the EP. The results are for $\alpha = 0.2$, purple (right-hand side) EPs. Similar results are obtained, with appropriate long-time windows, for left- and right-side EP contours for all α . For the representative data shown, the power-law exponents are 2.62, 4.83, and 8.08, for $N = 2$, $N = 3$, and $N = 5$, respectively.

coupled RLC circuits with dynamic parameters to show that energy dynamics in it is generated by a $(3N - 1)$ -dimensional non-Hermitian Hamiltonian, and through general formalism, spelled out the constraints that make such Hamiltonian have chiral and \mathcal{PT} symmetry. We have then shown that this model, with $2N$ dynamical variables, can be mapped onto an N -dimensional tight-binding lattice that can support an EP of order N .

By implementing the gain and loss through a periodic variation of the inductances in the RLC units, we have numerically mapped out the Floquet \mathcal{PT} -phase diagram for two, three, and five oscillator chains, all of which show EP contours at vanishingly small non-Hermiticities. By tracking the circuit's energy, we are able extract the order of EP by looking

at the power-law-in-time exponent for the $E(t)$ increase. Our results will be useful for realizing robust, arbitrary-order EPs by means of complex gauge fields in dynamically modulated synthetical oscillator networks.

ACKNOWLEDGMENTS

This work was supported by DGAPA-UNAM under Project No. UNAM-PAPIIT IN101623, and by CONACYT under Project No. A1-S-8317. J.D.H.-M. thankfully acknowledges financial support by CONACYT. Y.N.J. is supported by ONR Grant No. N00014-21-1-2630.

APPENDIX: EXPLICIT HAMILTONIAN EXPRESSIONS FOR TWO, THREE, AND FIVE OSCILLATOR CIRCUITS

1. Two coupled RLC oscillators

For two coupled RLC oscillators, $|\phi(t)\rangle = (V_1, V_2, I_1, I_2, I_{x1})^T$ and the 5×5 matrix $H(t)$ with purely imaginary entries is given by

$$H(t) = i \begin{bmatrix} -\frac{1}{C_1 R_1} & 0 & -\frac{1}{C_1} & 0 & -\frac{1}{C_1} \\ 0 & -\frac{1}{C_2 R_2} & 0 & -\frac{1}{C_2} & \frac{1}{C_2} \\ \frac{1}{L_1(t)} & 0 & 0 & 0 & 0 \\ 0 & \frac{1}{L_2(t)} & 0 & 0 & 0 \\ \frac{1}{L_{x1}} & -\frac{1}{L_{x1}} & 0 & 0 & 0 \end{bmatrix}. \quad (\text{A1})$$

To generate balanced gain-loss through the temporal modulation of the inductors, we use $L_1(t) = L_0 e^{f(t)}$ and $L_2(t) = L_0 e^{-f(t)}$, and set $C_{1,2} = C_0$, $L_{x1} = 0.5L_0$, and $R_{1,2} = R_0$. With $\gamma(t) = df/dt$, the circuit Hamiltonian can be written as

$$H_{\text{cir}}(t) = i \begin{bmatrix} -\frac{1}{C_0 R_0} & 0 & -\frac{\omega_0}{e^{f(t)/2}} & 0 & -\frac{\omega_0}{\sqrt{0.5}} \\ 0 & -\frac{1}{C_0 R_0} & 0 & -\frac{\omega_0}{e^{-f(t)/2}} & \frac{\omega_0}{\sqrt{0.5}} \\ \frac{\omega_0}{e^{f(t)/2}} & 0 & \frac{\gamma(t)}{2} & 0 & 0 \\ 0 & \frac{\omega_0}{e^{-f(t)/2}} & 0 & -\frac{\gamma(t)}{2} & 0 \\ \frac{\omega_0}{\sqrt{0.5}} & -\frac{\omega_0}{\sqrt{0.5}} & 0 & 0 & 0 \end{bmatrix}. \quad (\text{A2})$$

2. Three coupled RLC oscillators

For three coupled RLC oscillators, $|\phi(t)\rangle = (V_1, V_2, V_3, I_1, I_2, I_3, I_{x1}, I_{x2})^T$, and the 8×8 matrix $H(t)$ with purely imaginary entries is given by

$$H(t) = i \begin{bmatrix} -\frac{1}{C_1 R_1} & 0 & 0 & -\frac{1}{C_1} & 0 & 0 & -\frac{1}{C_1} & 0 \\ 0 & -\frac{1}{C_2 R_2} & 0 & 0 & -\frac{1}{C_2} & 0 & \frac{1}{C_2} & -\frac{1}{C_2} \\ 0 & 0 & -\frac{1}{C_3 R_3} & 0 & 0 & -\frac{1}{C_3} & 0 & \frac{1}{C_3} \\ \frac{1}{L_1(t)} & 0 & 0 & 0 & 0 & 0 & 0 & 0 \\ 0 & \frac{1}{L_2} & 0 & 0 & 0 & 0 & 0 & 0 \\ 0 & 0 & \frac{1}{L_3(t)} & 0 & 0 & 0 & 0 & 0 \\ \frac{1}{L_{x1}} & -\frac{1}{L_{x1}} & 0 & 0 & 0 & 0 & 0 & 0 \\ 0 & \frac{1}{L_{x2}} & -\frac{1}{L_{x2}} & 0 & 0 & 0 & 0 & 0 \end{bmatrix}. \quad (\text{A3})$$

To maintain \mathcal{PT} symmetry and generate balanced gain and loss, we use $L_{x1} = L_{x2} = 0.5L_0$, $L_1(t) = L_0e^{f(t)}$, $L_2 = L_0$, and $L_3(t) = L_0e^{-f(t)}$. The resulting circuit Hamiltonian becomes

$$H_{\text{cir}}(t) = i \begin{bmatrix} -\frac{1}{C_0R_0} & 0 & 0 & -\frac{\omega_0}{e^{f(t)/2}} & 0 & 0 & -\frac{\omega_0}{\sqrt{0.5}} & 0 \\ 0 & -\frac{1}{C_0R_0} & 0 & 0 & -\omega_0 & 0 & \frac{\omega_0}{\sqrt{0.5}} & -\frac{\omega_0}{\sqrt{0.5}} \\ 0 & 0 & -\frac{1}{C_0R_0} & 0 & 0 & -\frac{\omega_0}{e^{-f(t)/2}} & 0 & \frac{\omega_0}{\sqrt{0.5}} \\ \frac{\omega_0}{e^{f(t)/2}} & 0 & 0 & \gamma(t) & 0 & 0 & 0 & 0 \\ 0 & \omega_0 & 0 & 0 & 0 & 0 & 0 & 0 \\ 0 & 0 & \frac{\omega_0}{e^{-f(t)/2}} & 0 & 0 & -\gamma(t) & 0 & 0 \\ \frac{\omega_0}{\sqrt{0.5}} & -\frac{\omega_0}{\sqrt{0.5}} & 0 & 0 & 0 & 0 & 0 & 0 \\ 0 & \frac{\omega_0}{\sqrt{0.5}} & -\frac{\omega_0}{\sqrt{0.5}} & 0 & 0 & 0 & 0 & 0 \end{bmatrix}. \quad (\text{A4})$$

3. Five coupled RLC oscillators

For $N = 5$, the 14-dimensional state vector is $|\phi(t)\rangle = (V_1, V_2, V_3, V_4, V_5, I_1, I_2, I_3, I_4, I_5, I_{x1}, I_{x2}, I_{x3}, I_{x4})^T$ and the 14-dimensional, purely imaginary matrix $H(t)$ becomes

$$H(t) = i \begin{bmatrix} -\frac{1}{C_1R_1} & 0 & 0 & 0 & 0 & -\frac{1}{C_1} & 0 & 0 & 0 & 0 & -\frac{1}{C_1} & 0 & 0 & 0 \\ 0 & -\frac{1}{C_2R_2} & 0 & 0 & 0 & 0 & -\frac{1}{C_2} & 0 & 0 & 0 & \frac{1}{C_2} & -\frac{1}{C_2} & 0 & 0 \\ 0 & 0 & -\frac{1}{C_3R_3} & 0 & 0 & 0 & 0 & -\frac{1}{C_3} & 0 & 0 & 0 & \frac{1}{C_3} & -\frac{1}{C_3} & 0 \\ 0 & 0 & 0 & -\frac{1}{C_4R_4} & 0 & 0 & 0 & 0 & -\frac{1}{C_4} & 0 & 0 & 0 & \frac{1}{C_4} & -\frac{1}{C_4} \\ 0 & 0 & 0 & 0 & -\frac{1}{C_5R_5} & 0 & 0 & 0 & 0 & -\frac{1}{C_5} & 0 & 0 & 0 & \frac{1}{C_5} \\ \frac{1}{L_1(t)} & 0 & 0 & 0 & 0 & 0 & 0 & 0 & 0 & 0 & 0 & 0 & 0 & 0 \\ 0 & \frac{1}{L_2(t)} & 0 & 0 & 0 & 0 & 0 & 0 & 0 & 0 & 0 & 0 & 0 & 0 \\ 0 & 0 & \frac{1}{L_3} & 0 & 0 & 0 & 0 & 0 & 0 & 0 & 0 & 0 & 0 & 0 \\ 0 & 0 & 0 & \frac{1}{L_4(t)} & 0 & 0 & 0 & 0 & 0 & 0 & 0 & 0 & 0 & 0 \\ 0 & 0 & 0 & 0 & \frac{1}{L_5(t)} & 0 & 0 & 0 & 0 & 0 & 0 & 0 & 0 & 0 \\ \frac{1}{L_{x1}} & -\frac{1}{L_{x1}} & 0 & 0 & 0 & 0 & 0 & 0 & 0 & 0 & 0 & 0 & 0 & 0 \\ 0 & \frac{1}{L_{x2}} & -\frac{1}{L_{x2}} & 0 & 0 & 0 & 0 & 0 & 0 & 0 & 0 & 0 & 0 & 0 \\ 0 & 0 & \frac{1}{L_{x3}} & -\frac{1}{L_{x3}} & 0 & 0 & 0 & 0 & 0 & 0 & 0 & 0 & 0 & 0 \\ 0 & 0 & 0 & \frac{1}{L_{x4}} & -\frac{1}{L_{x4}} & 0 & 0 & 0 & 0 & 0 & 0 & 0 & 0 & 0 \end{bmatrix}. \quad (\text{A5})$$

To create \mathcal{PT} -symmetric circuit with balanced gain and loss, we use $L_{x1} = 0.67L_0 = L_{x4}$, $L_{x2} = 0.5L_0 = L_{x3}$. The time-dependent inductors vary as $L_{1,5}(t) = L_0e^{\pm 2f(t)}$, $L_{2,4}(t) = L_0e^{\pm f(t)}$, and $L_3 = L_0$. This leads to a 14×14 circuit Hamiltonian with purely imaginary entries,

$$H_{\text{cir}}(t) = i \begin{bmatrix} -\frac{1}{C_0R_0} & 0 & 0 & 0 & 0 & -\frac{\omega_0}{e^{f(t)}} & 0 & 0 & 0 & 0 & -\frac{\omega_0}{\sqrt{0.67}} & 0 & 0 & 0 \\ 0 & -\frac{1}{C_0R_0} & 0 & 0 & 0 & 0 & -\frac{\omega_0}{e^{f(t)/2}} & 0 & 0 & 0 & \frac{\omega_0}{\sqrt{0.67}} & -\frac{\omega_0}{\sqrt{0.5}} & 0 & 0 \\ 0 & 0 & -\frac{1}{C_0R_0} & 0 & 0 & 0 & 0 & -\omega_0 & 0 & 0 & 0 & \frac{\omega_0}{\sqrt{0.5}} & -\frac{\omega_0}{\sqrt{0.5}} & 0 \\ 0 & 0 & 0 & -\frac{1}{C_0R_0} & 0 & 0 & 0 & 0 & -\frac{\omega_0}{e^{-f(t)/2}} & 0 & 0 & 0 & \frac{\omega_0}{\sqrt{0.5}} & -\frac{\omega_0}{\sqrt{0.67}} \\ 0 & 0 & 0 & 0 & -\frac{1}{C_0R_0} & 0 & 0 & 0 & 0 & -\frac{\omega_0}{e^{-f(t)}} & 0 & 0 & 0 & \frac{\omega_0}{\sqrt{0.67}} \\ \frac{\omega_0}{e^{f(t)}} & 0 & 0 & 0 & 0 & 2\gamma(t) & 0 & 0 & 0 & 0 & 0 & 0 & 0 & 0 \\ 0 & \frac{\omega_0}{e^{f(t)/2}} & 0 & 0 & 0 & 0 & \gamma(t) & 0 & 0 & 0 & 0 & 0 & 0 & 0 \\ 0 & 0 & \omega_0 & 0 & 0 & 0 & 0 & 0 & 0 & 0 & 0 & 0 & 0 & 0 \\ 0 & 0 & 0 & \frac{\omega_0}{e^{-f(t)/2}} & 0 & 0 & 0 & 0 & -\gamma(t) & 0 & 0 & 0 & 0 & 0 \\ 0 & 0 & 0 & 0 & \frac{\omega_0}{e^{-f(t)}} & 0 & 0 & 0 & 0 & -2\gamma(t) & 0 & 0 & 0 & 0 \\ \frac{\omega_0}{\sqrt{0.67}} & -\frac{\omega_0}{\sqrt{0.67}} & 0 & 0 & 0 & 0 & 0 & 0 & 0 & 0 & 0 & 0 & 0 & 0 \\ 0 & \frac{\omega_0}{\sqrt{0.5}} & -\frac{\omega_0}{\sqrt{0.5}} & 0 & 0 & 0 & 0 & 0 & 0 & 0 & 0 & 0 & 0 & 0 \\ 0 & 0 & \frac{\omega_0}{\sqrt{0.5}} & -\frac{\omega_0}{\sqrt{0.5}} & 0 & 0 & 0 & 0 & 0 & 0 & 0 & 0 & 0 & 0 \\ 0 & 0 & 0 & \frac{\omega_0}{\sqrt{0.67}} & -\frac{\omega_0}{\sqrt{0.67}} & 0 & 0 & 0 & 0 & 0 & 0 & 0 & 0 & 0 \end{bmatrix}. \quad (\text{A6})$$

- [1] C. M. Bender and S. Boettcher, Real Spectra in non-Hermitian Hamiltonians having \mathcal{PT} Symmetry, *Phys. Rev. Lett.* **80**, 5243 (1998).
- [2] C. M. Bender, S. Boettcher, and P. N. Meisinger, \mathcal{PT} -symmetric quantum mechanics, *J. Math. Phys.* **40**, 2201 (1999).
- [3] C. M. Bender, Introduction to \mathcal{PT} -symmetric quantum theory, *Contemp. Phys.* **46**, 277 (2005).
- [4] G. Lévai and M. Znojil, Systematic search for \mathcal{PT} -symmetric potentials with real energy spectra, *J. Phys. A: Math. Gen.* **33**, 7165 (2000).
- [5] J. D. Huerta Morales, J. Guerrero, S. López-Aguayo, and B. M. Rodríguez-Lara, Revisiting the optical \mathcal{PT} -symmetric dimer, *Symmetry* **8**, 83 (2016).
- [6] A. Guo, G. J. Salamo, D. Duchesne, R. Morandotti, M. Volatier-Ravat, V. Aimez, G. A. Siviloglou, and D. N. Christodoulides, Observation of \mathcal{PT} -Symmetry Breaking in Complex Optical Potentials, *Phys. Rev. Lett.* **103**, 093902 (2009).
- [7] C. E. Rüter, K. G. Makris, R. El-Ganainy, D. N. Christodoulides, M. Segev, and D. Kip, Observation of parity–time symmetry in optics, *Nat. Phys.* **6**, 192 (2010).
- [8] L. Feng, R. El-Ganainy, and L. Ge, Non-Hermitian photonics based on parity–time symmetry, *Nat. Photonics* **11**, 752 (2017).
- [9] R. El-Ganainy, K. G. Makris, M. Khajavikhan, Z. H. Musslimani, S. Rotter, and D. N. Christodoulides, Non-Hermitian physics and \mathcal{PT} symmetry, *Nat. Phys.* **14**, 11 (2018).
- [10] H. Eleuch and I. Rotter, Clustering of exceptional points and dynamical phase transitions, *Phys. Rev. A* **93**, 042116 (2016).
- [11] S. K. Özdemir, S. Rotter, F. Nori, and L. Yang, Parity–time symmetry and exceptional points in photonics, *Nat. Mater.* **18**, 783 (2019).
- [12] M. Sakhdari, M. Hajizadegan, Q. Zhong, D. N. Christodoulides, R. El-Ganainy, and P.-Y. Chen, Experimental Observation of \mathcal{PT} Symmetry Breaking Near Divergent Exceptional Points, *Phys. Rev. Lett.* **123**, 193901 (2019).
- [13] H. Hodaie, A. U. Hassan, S. Wittek, H. Garcia-Gracia, R. El-Ganainy, D. N. Christodoulides, and M. Khajavikhan, Enhanced sensitivity at higher-order exceptional points, *Nature (London)* **548**, 187 (2017).
- [14] W. Chen, S. K. Özdemir, G. Zhao, J. Wiersig, and L. Yang, Exceptional points enhance sensing in an optical microcavity, *Nature (London)* **548**, 192 (2017).
- [15] Y. Huang, Y. Shen, and G. Veronis, Non- \mathcal{PT} -symmetric two-layer cylindrical waveguide for exceptional-point-enhanced optical devices, *Opt. Express* **27**, 37494 (2019).
- [16] M. I. Rosa, M. Mazzotti, and M. Ruzzene, Exceptional points and enhanced sensitivity in \mathcal{PT} -symmetric continuous elastic media, *J. Mech. Phys. Solids* **149**, 104325 (2021).
- [17] I. Rotter, A non-Hermitian Hamilton operator and the physics of open quantum systems, *J. Phys. A: Math. Theor.* **42**, 153001 (2009).
- [18] M. Müller and I. Rotter, Exceptional points in open quantum systems, *J. Phys. A: Math. Theor.* **41**, 244018 (2008).
- [19] M. H. Teimourpour, Q. Zhong, M. Khajavikhan, and R. El-Ganainy, Higher Order Exceptional Points in Discrete Photonics Platforms, *Springer Tracts Mod. Phys.* **280**, 261 (2018).
- [20] W. D. Heiss, The physics of exceptional points, *J. Phys. A: Math. Theor.* **45**, 444016 (2012).
- [21] M. A. Quiroz-Juárez, A. Perez-Leija, K. Tschernig, B. M. Rodríguez-Lara, O. S. Magaña-Loaiza, K. Busch, Y. N. Joglekar, and R. de J. León-Montiel, Exceptional points of any order in a single, lossy waveguide beam splitter by photon-number-resolved detection, *Photon. Res.* **7**, 862 (2019).
- [22] S. M. Zhang, X. Z. Zhang, L. Jin, and Z. Song, High-order exceptional points in supersymmetric arrays, *Phys. Rev. A* **101**, 033820 (2020).
- [23] M. Y. Nada and F. Capolino, Exceptional point of sixth-order degeneracy in a modified coupled-resonator optical waveguide, *J. Opt. Soc. Am. B* **37**, 2319 (2020).
- [24] J. Wiersig, Enhancing the Sensitivity of Frequency and Energy Splitting Detection by Using Exceptional Points: Application to Microcavity Sensors for Single-Particle Detection, *Phys. Rev. Lett.* **112**, 203901 (2014).
- [25] Z. P. Liu, J. Zhang, S. K. Özdemir, B. Peng, H. Jing, X. Y. Lü, C. W. Li, L. Yang, F. Nori, and Y. X. Liu, Metrology with \mathcal{PT} -Symmetric Cavities: Enhanced Sensitivity Near the \mathcal{PT} -Phase Transition, *Phys. Rev. Lett.* **117**, 110802 (2016).
- [26] N. Moiseyev and M. Šindelka, Transfer of information through waveguides near an exceptional point, *Phys. Rev. A* **103**, 033518 (2021).
- [27] B. Peng, S. K. Özdemir, F. Lei, F. Monifi, M. Gianfreda, G. L. Long, S. Fan, F. Nori, C. M. Bender, and L. Yang, Parity–time-symmetric whispering-gallery microcavities, *Nat. Phys.* **10**, 394 (2014).
- [28] H. Jing, S. K. Özdemir, H. Lü, and F. Nori, High-order exceptional points in optomechanics, *Sci. Rep.* **7**, 3386 (2017).
- [29] B. Jaramillo Ávila, C. Ventura-Velázquez, R. de J. León-Montiel, Y. N. Joglekar, and B. M. Rodríguez-Lara, \mathcal{PT} -symmetry from Lindblad dynamics in a linearized optomechanical system, *Sci. Rep.* **10**, 1761 (2020).
- [30] W. Xiong, Z. Li, Y. Song, J. Chen, G. Q. Zhang, and M. Wang, Higher-order exceptional point in a pseudo-Hermitian cavity optomechanical system, *Phys. Rev. A* **104**, 063508 (2021).
- [31] F. Quijandría, U. Naether, S. K. Özdemir, F. Nori, and D. Zueco, \mathcal{PT} -symmetric circuit QED, *Phys. Rev. A* **97**, 053846 (2018).
- [32] Z. Bian, L. Xiao, K. Wang, X. Zhan, F. A. Onanga, F. Ruzicka, W. Yi, Y. N. Joglekar, and P. Xue, Conserved quantities in parity-time symmetric systems, *Phys. Rev. Res.* **2**, 022039(R) (2020).
- [33] C. Shi, M. Dubois, Y. Chen, L. Cheng, H. Ramezani, Y. Wang, and X. Zhang, Accessing the exceptional points of parity-time symmetric acoustics, *Nat. Commun.* **7**, 11110 (2016).
- [34] K. Ding, G. Ma, M. Xiao, Z. Q. Zhang, and C. T. Chan, Emergence, Coalescence, and Topological Properties of Multiple Exceptional Points and Their Experimental Realization, *Phys. Rev. X* **6**, 021007 (2016).
- [35] S. Wang, B. Hou, W. Lu, Y. Chen, Z. Q. Zhang, and C. T. Chan, Arbitrary order exceptional point induced by photonic spin–orbit interaction in coupled resonators, *Nat. Commun.* **10**, 832 (2019).
- [36] J. Schindler, A. Li, M. C. Zheng, F. M. Ellis, and T. Kottos, Experimental study of active LRC circuits with \mathcal{PT} symmetries, *Phys. Rev. A* **84**, 040101(R) (2011).
- [37] Z. Lin, J. Schindler, F. M. Ellis, and T. Kottos, Experimental observation of the dual behavior of \mathcal{PT} -symmetric scattering, *Phys. Rev. A* **85**, 050101(R) (2012).
- [38] H. Kazemi, M. Y. Nada, T. Mealy, A. F. Abdelshafy, and F. Capolino, Exceptional Points of Degeneracy Induced by Linear Time-Periodic Variation, *Phys. Rev. Appl.* **11**, 014007 (2019).

- [39] H. Kazemi, M. Y. Nada, A. Nikzamir, F. Maddaleno, and F. Capolino, Experimental demonstration of exceptional points of degeneracy in linear time periodic systems and exceptional sensitivity, *J. Appl. Phys.* **131**, 144502 (2022).
- [40] A. Stegmaier, S. Imhof, T. Helbig, T. Hofmann, C. H. Lee, M. Kremer, A. Fritzsche, T. Feichtner, S. Klemmt, S. Höfling, I. Boettcher, I. C. Fulga, L. Ma, O. G. Schmidt, M. Greiter, T. Kiessling, A. Szameit, and R. Thomale, Topological Defect Engineering and \mathcal{PT} Symmetry in non-Hermitian Electrical Circuits, *Phys. Rev. Lett.* **126**, 215302 (2021).
- [41] X. Yang, J. Li, Y. Ding, M. Xu, X.-F. Zhu, and J. Zhu, Observation of Transient Parity-Time Symmetry in Electronic Systems, *Phys. Rev. Lett.* **128**, 065701 (2022).
- [42] W. Cao, C. Wang, W. Chen, S. Hu, H. Wang, L. Yang, and X. Zhang, Fully integrated parity-time-symmetric electronics, *Nat. Nanotechnol.* **17**, 262 (2022).
- [43] M. A. Quiroz-Juárez, K. S. Agarwal, Z. A. Cochran, J. L. Aragón, Y. N. Joglekar, and R. J. León-Montiel, On-Demand Parity-Time Symmetry in a Lone Oscillator through Complex Synthetic Gauge Fields, *Phys. Rev. Appl.* **18**, 054034 (2022).
- [44] Y. N. Joglekar, C. Thompson, D. D. Scott, and G. Vemuri, Optical waveguide arrays: quantum effects and \mathcal{PT} symmetry breaking, *Eur. Phys. J. Appl. Phys.* **63**, 30001 (2013).
- [45] A. Perez-Leija, R. Keil, H. Moya-Cessa, A. Szameit, and D. N. Christodoulides, Perfect transfer of path-entangled photons in J_x photonic lattices, *Phys. Rev. A* **87**, 022303 (2013).
- [46] S. Weimann, A. Perez-Leija, M. Lebugle, R. Keil, M. Tichy, M. Gräfe, R. Heilmann, S. Nolte, H. Moya-Cessa, G. Weihs, D. N. Christodoulides, and A. Szameit, Implementation of quantum and classical discrete fractional Fourier transforms, *Nat. Commun.* **7**, 11027 (2016).
- [47] M. A. Quiroz-Juárez, C. You, J. Carrillo-Martínez, D. Montiel-Álvarez, J. L. Aragón, O. S. Magaña-Loaiza, and R. J. León-Montiel, Reconfigurable network for quantum transport simulations, *Phys. Rev. Res.* **3**, 013010 (2021).
- [48] K. Tschernig, R. de J. León-Montiel, O. S. Magaña-Loaiza, A. Szameit, K. Busch, and A. Perez-Leija, Multiphoton discrete fractional Fourier dynamics in waveguide beam splitters, *J. Opt. Soc. Am. B* **35**, 1985 (2018).
- [49] R. de J. León-Montiel, M. A. Quiroz-Juárez, J. L. Domínguez-Juárez, R. Quintero-Torres, J. L. Aragón, A. K. Harter, and Y. N. Joglekar, Observation of slowly decaying eigenmodes without exceptional points in Floquet dissipative synthetic circuits, *Commun. Phys.* **1**, 88 (2018).
- [50] Y. N. Joglekar, R. Marathe, P. Durganandini, and R. K. Pathak, \mathcal{PT} spectroscopy of the Rabi problem, *Phys. Rev. A* **90**, 040101(R) (2014).